Materials Advances

ROYAL SOCIETY OF CHEMISTRY

PAPER

View Article Online
View Journal | View Issue

Cite this: *Mater. Adv.*, 2022, 3, 7339

Green-light-emitting carbon dots *via* eco-friendly route and their potential in ferric-ion detection and WLEDs†

Hanxun Qiu, Fangyu Yuan, Yuanchi Wang, Zheng Zhang, Jing Li and Ying Li *

As a rising star in the carbon family, carbon dots (CDs) have been attracting tremendous interest in the scientific community by virtue of their unique physicochemical, optical, and electronic properties. In particular, CDs in the solid state are strongly desired for their potential applications in light-emitting devices due to their simplicity of preparation and enhanced photoluminescence (PL) performance. Fortunately, a microwave-assisted solvent-free approach is proposed here for the first time to rapidly obtain green-light-emitting carbon dots (G-CDs). G-CDs with a maximum emission wavelength of 521 nm were achieved, for which the photoluminescence quantum yield and production yield are as high as 48.8% and 59.15%, respectively. Moreover, the G-CDs have a uniform size distribution, and good thermal and pH stability, enabling the highly sensitive detection of Fe^{3+} with a limit as low as 10 μM and potential in CD-based white-light-emitting diodes (WLEDs). Typically, the G-CD-based WLEDs favorably emit white light with a color rendering index of 92.2 and Commission internationale de l'éclairage (CIE) coordinates of (0.3437, 0.3358), demonstrating good color chromatic stability. On account of its environmental friendliness, simplicity, high efficiency, and low cost, this approach is promising for the scaled-up production of CDs, and may promote their application in detection sensors and high-performance light-emitting devices.

Received 9th May 2022,
Accepted 23rd July 2022

DOI: 10.1039/d2ma00520d

rsc.li/materials-advances

1. Introduction

Carbon materials are playing significant roles in the development of materials science. Most recently, as a new member of the carbon family, carbon dots (CDs) have emerged and aroused research hotspots in many fields, including biomedicine,[1,2] chemical sensors,[3–6] photocatalysis[7,8] and photoelectric devices,[9,10] due to their excellent and tunable fluorescence properties, abundant low-cost sources, low toxicity, appreciable biocompatibility and high thermal stability. In particular, the rich optical and electronic properties of CDs, which include tunable photoluminescence (PL),[11] extraordinary up-converted PL[12] and outstanding photo-induced electron transfer,[13] have attracted considerable interest in the photoelectric applications of white-light-emitting diodes (WLEDs).[14–16] Currently, commercial white-light-emitting fluorescent materials cannot be produced without rare-earth elements.[17] However, the non-renewable nature of rare-earth resources and the environmental pollution induced during the preparation processes have triggered many economic and environmental issues.[15] Therefore, it is of urgency to seek and develop low-cost and eco-friendly fluorescent materials with an efficient, stable and high-quality emission performance.

Being a new type of zero-dimensional (0D) fluorescent nanomaterial, CDs can be treated as a conjugated carbon nucleus with surface functional groups that primarily contain C, H and O elements, probably doped with heteroatoms such as B, N, S, F, P and Cl.[18–20] Precursors for CDs come from a wide range of sources and the preparation costs are less expensive. Moreover, CD characteristics include wide emission spectra, adjustable fluorescence, good thermal stability and low cytotoxicity, and are thus regarded as an ideal alternative for traditional rare-earth fluorescent materials.

So far, a series of synthesis routes have been developed for the controllable preparation of CDs since their discovery.[21] The preparation of CDs is generally divided into two categories of 'top-down' and 'bottom-up'. Top-down approaches aim to 'cut' graphene, carbon nanotubes and bituminous coal into small-sized CDs *via* electrochemical stripping,[22] chemical oxidation,[23] laser ablation[24] and ultrasonic synthesis.[25,26] By contrast, the

School of Materials and Chemistry, University of Shanghai for Science and Technology, Shanghai 200093, China. E-mail: liying@usst.edu.cn; Fax: +86-21-55270632; Tel: +86-21-55270632

† Electronic supplementary information (ESI) available. See DOI: https://doi.org/10.1039/d2ma00520d

bottom-up approaches synthesize CDs from carbon- and nitrogen-containing precursors through pyrolysis, carbonization or polymerization under hydrothermal,[27] solvothermal,[28] and microwave-assisted hydrothermal processes.[29–31] Compared with top-down approaches, bottom-up techniques can make it more possible to fabricate CDs with a relatively uniform structure and an excellent performance. Therefore, hydro/solvothermal approaches have been extensively employed for studies on CDs most recently. The introduction of microwave irradiation to the synthesis approaches further endowed the fabrication of CDs with enhanced reaction rates, increased product yields, easy size control, and improved uniformity.[32] Unfortunately, organic solvents or liquid reagents are inevitably employed during the process to dissolve the precursors, to increase the probability of particle collisions for fuller conversion.

Liu *et al.*[33] synthesized three kinds of CD with different PL (blue, yellow, and orange) *via* microwave-assisted heating. These CDs displayed wavelength-independent excitation and similar fluorescence lifetimes, suggesting the potential for multicolor imaging of cells and light-emitting diodes (LEDs). Sun and co-workers[34] employed a microwave-assisted solvothermal method for the preparation of highly efficient red-emitting CDs, which presented low toxicity, high stability and a high photothermal conversion efficiency, and a 22.9% PL quantum yield (QY). However, this progress could not conceal the limitations of the approaches, specifically complicated procedures, tedious post-treatments, unavailability in scaled-up production, the production of organic effluents, and confinement to direct use for light-emitting devices. Therefore, a more facile, efficient, eco-friendly, and solvent-free method is still strongly desired by the scientific community. So far, microwave-assisted solid-phase approaches for the preparation of CDs have been rarely reported, where a few have concentrated on blue-light-emitting CDs but with relatively low yields. In a previous report by Wang *et al.*[35] citric acid and glutathione were employed as the reagents to produce CDs with blue-light emission (440 nm) *via* microwave-assisted solid-phase synthesis, with a production yield of 35 ± 3%. Recently, Cao's group[36] reported the synthesis of N-CDs with blue-light emission (484 nm) using a solvent-free microwave-assisted method. The as-prepared N-CDs exhibited excellent dispersibility, with a QY of 38.88%, and characteristics of excitation- and concentration-dependence. It is well known that short-wavelength light-emitting CDs may limit the absorption and conversion ability of light, restricting their applications in biological imaging, LEDs and other fields. Therefore, CDs that emit green, yellow, and red light with long wavelengths are of great significance for extending the light-absorption ranges and realizing the effective utilization of light. However, there have been few reports so far on CDs with longer wavelength light emission that are produced *via* microwave-assisted solid-phase routes.

Herein, we report that CDs with a much longer wavelength emission, *i.e.*, green light-emitting CDs (G-CDs), were obtained *via* a microwave-assisted solid-phase reaction. The emission range covered the whole green-light region, and the favored maximum emission peak is located at 521 nm. The QY and production yield were as high as 48.8% and 59.15%, respectively, which is much higher than previously reported using a microwave-assisted solvothermal method. Moreover, just a few minutes were required for the entire process, implying the highly efficient preparation of G-CDs. It is worth noting that the superior dispersion of G-CDs shows great potential for use as a chemical sensor to monitor the concentration of Fe^{3+} with a high detection sensitivity. Besides, a WLED fabricated with the as prepared G-CDs performs with a color rendering index (CRI) of 92.2 and Commission internationale de l'éclairage (CIE) coordinates of (0.3437, 0.3358), which are very close to the pure white-light CRI of 100 and CIE coordinates (0.33, 0.33). Compared with microwave-assisted wet chemical synthesis, this approach avoids the use of toxic organic reactive solvents, and simplifies the post-treatment procedures. Therefore, this finding enables the potential scaled-up production of CDs, rendering great promise for G-CDs in the field of white-light emission.

2. Experimental

2.1. Materials and chemicals

Citric acid, ethanol, urea, and starch were purchased from Sinopharm Chemical Reagent Co., Ltd (Shanghai, China). Commercially available GaN-LED chips (440 nm) and red phosphor (N630) were purchased from Zhanwanglong Science and Technology Co., Ltd (Shenzhen, China). Epoxy resin (Araldite resin 2020A/2020B) was supplied by HUNTSMAN (Shanghai, China). All chemicals used were of analytical grade and as received without any further purification. Deionized water was used in all experiments (prepared in our laboratory).

2.2. Preparation of G-CDs

The preparation process for the G-CDs is shown in Scheme 1. Typically, a solid-state mixture of 100 mg citric acid and 300 mg urea was ground to a fine powder using an agate mortar, then was transferred to a 10 ml microwave tube and heated at 190 °C for 8 min in a microwave reactor (CEM) operated in the standard mode. After the reaction, the excess urea attached to the tube wall was removed, and the remaining solid powder was collected. Subsequently, 500 mL of ethanol was added to the solid mixture, followed by ultrasonication for 3 h. Interestingly, almost all solids could be completely dispersed if sufficient ethanol was used, indicating that the resulting materials were composed of dispersible CDs. The dispersion was stored at room temperature for subsequent testing (Scheme 1).

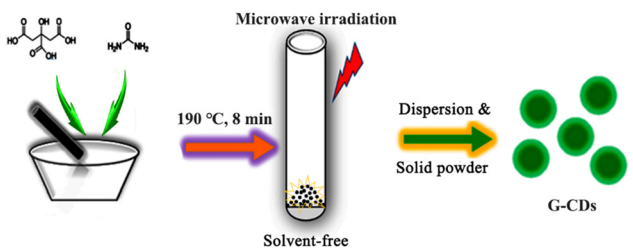

Scheme 1 Schematic of the preparation process for the G-CDs.

2.3. Fabrication of G-CD-based WLEDs

Typically, 15 mL of the G-CD dispersion and 50 mg of starch were mixed and stirred for 48 h. After vacuum filtration with a 0.22 μm membrane, the obtained precipitate was dried at 60 °C for 8 h to obtain the G-CD-based phosphor. Then both the phosphor and the commercial nitride red phosphor were added to epoxy resin and stirred sufficiently until the bubbles had disappeared. Finally, the mixture was coated on a commercial GaN-LEDs chip (460 nm) and dried at 120 °C for 2 h. The thus-fabricated devices would then be tested to assess their performance.

2.4. Fe^{3+} detection

The detection of Fe^{3+} ions was performed using PBS (pH = 7.4) buffer solution. In a typical assay, the G-CD (10 μL) dispersion was added to PBS buffer solution (4 mL), followed by the addition of different Fe^{3+}-ion concentrations (1, 5, 10, 20, 40, 50, 100, and 200 μM). PL characterization was performed at 420 nm after reaction for 10 min. The selectivity for Fe^{3+} was confirmed by adding other metal-ion (Zn^{2+}, Pb^{2+}, Ni^{2+}, Mn^{2+}, Mg^{2+}, K^{+}, Co^{2+}, Cd^{2+}, Ag^{+}, or Cu^{2+}) solutions in a similar way. All experiments were performed at room temperature.

2.5. Measurement of fluorescence QY

The QY was determined using the reference point method. Rhodamine 6G (ethanol solution as solvent, QY = 95%) was chosen as the standard.

$$\Phi_s = \Phi_r \times \frac{I_s}{I_r} \times \frac{A_r}{A_s} \times \frac{n_s^2}{n_r^2} \quad (1)$$

Here in eqn (1), Φ represents the QY, I is the emission peak area, A is the absorption intensity, and n is the refractive index of the solution. The subscript s denotes the sample to be tested, and r denotes the standard sample. In order to minimize reabsorption effects, the absorption in the 10 mm fluorescence cuvettes used was kept below 0.05 at the excitation wavelength (365–460 nm).

2.6. Estimation of production yield

Surprisingly, all the reaction products could be well dispersed in sufficient ethanol *via* full ultrasonic treatment. Typically, 20 mL of the obtained CD dispersion was dried until the weight remained constant. Accordingly, the concentration of the G-CD ethanol dispersion could be estimated to deduce the production yield (ratio of the mass of the product to that of the reactant).

2.7. Characterization

Transmission electron microscopy (TEM) images were observed using a field-emission electron microscope (TECNAI G2) with a 300 kV electron voltage. The average size of the CDs was obtained by counting 200 individual particles in the TEM images. X-ray photoelectron spectra (XPS) were examined using a spectrometer (Physical Electronics PHI-5300) with a Sigma probe and monochromatic Mg Kα radiation at a power of 250 W and a voltage of 14 kV. The Fourier transform infrared (FTIR) spectra were recorded at room temperature using an FTIR spectrometer (PerkinElmer, Spectrum 100), and the UV-vis absorption spectra were obtained using a spectrophotometer (PerkinElmer, Lam 750). The PL emission spectra were measured using a fluorescence spectrometer (Keithley, F-4000). The fluorescence lifetime was measured using a steady-state/transient fluorescence spectrometer (Edinburgh, FLS1000) at an excitation wavelength of 440 nm and an emission wavelength of 521 nm. For UV-Vis and PL characterization, the samples were diluted in dispersion with a concentration of 0.06 mg mL^{-1}, ensuring that the absorbance was less than unity at 365 nm. The electro-optical characteristics of the WLEDs were evaluated using an automatic temperature-controlled LED electro-optical analyzer (ATA-1000, 350–1100 nm). The WLEDs work with a forward bias current of 20 mA.

3. Results and discussion

3.1. Composition and structure of G-CDs

Green-light-emitting CDs were synthesized using critic and urea as the starting materials through a facile solvent-free microwave-assisted solid-phase reaction process, as illustrated in Scheme 1. The resulting G-CDs exhibit bright green fluorescence with a maximum excitation/emission at 440/521 nm.

The morphology and structure of the as-prepared G-CDs were investigated using TEM. As shown in Fig. 1(a), the G-CDs highlighted in dark dots are well dispersed in the form of spherical nanoparticles with no agglomeration and cross-linking, indicating the successful synthesis of G-CDs *via* the microwave-assisted solid-phase reaction. The high-resolution (HR) TEM image provided in the inset further confirms that the CDs exhibit well-resolved fringes with a lattice spacing of 0.21 nm, which corresponds to the (100) in-plane crystallographic facet of graphitic carbon. Fig. 1(b) shows the Gaussian size distribution and histogram of the G-CDs. Typically, the diameter ranges predominantly from 2.7 to 4.7 nm, and the average particle size is approximately 3.8 ± 0.25 nm (Fig. 1).

The surface functional groups and chemical composition of the G-CDs were identified *via* their FTIR and XPS spectra. The FTIR spectrum of the as-prepared CDs shown in Fig. 1(c) presents three strong peaks centered at 1256 cm^{-1}, 1528 cm^{-1} and 1720 cm^{-1}, which are attributed to the stretching vibrations of C–O, C═C and C═O, respectively. The peaks around 3430 cm^{-1} and 2960 cm^{-1} are ascribed to vibrations of –OH and $–CH_2$, respectively. This indicates that there are abundant oxygen/hydrogen-containing functional groups on CD surface, which endows the G-CDs with outstanding dispersibility in aqueous solution. Moreover, two peaks located at 1500 cm^{-1} and 3200 cm^{-1} correspond to the stretching vibrations of C–N═ and N–H, respectively, suggesting that the element N was successfully hybridized in the G-CDs. As has previously been stated,[11,33] variations in surface states and N content may lead to the tunable PL mechanism. An excellent luminescence performance would therefore be expected from the prepared G-CDs.

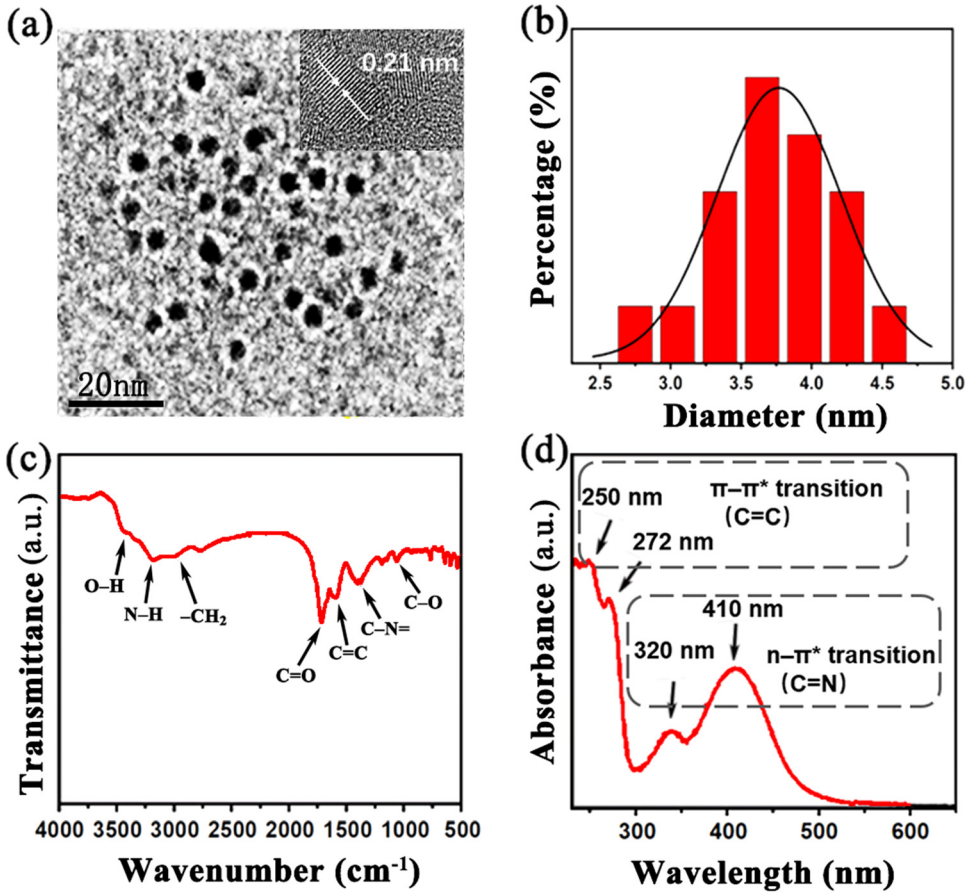

Fig. 1 (a) TEM and HRTEM images of well dispersed G-CDs; (b) Gaussian size distribution and histogram of G-CDs; (c) FTIR spectrum of the as-prepared G-CDs; and (d) UV-vis spectrum of G-CDs.

XPS was employed to further determine the composition of the G-CDs. As shown in Fig. 2(a), the XPS spectra reveal that the as-prepared G-CDs consist of three elements, *i.e.*, carbon, nitrogen, and oxygen, with contents of 51.07%, 23.66% and 25.28%, respectively. The high proportion of nitrogen indicates G-CDs are rich in nitrogen doping. Three obvious spectral peaks at 284.4 eV, 400.1 eV and 531.1 eV correspond to C 1s, N 1s and O 1s, respectively. Fig. 2(b) shows the C 1s spectra that are deconvoluted into four peaks at 284.5 eV (C═C or C–C), 285.4 eV (C–N or C–O), 288.1 (C═O) and 290.1 eV (O–C═O), indicating the different bonding types of the C atoms.[37] The high-resolution XPS spectra for N 1s presented in Fig. 2(c) can be deconvoluted into signals for the predominant pyrrolic or pyridinic N (*ca.* 399.4 eV), quaternary N (*ca.* 400.0 eV) and N-oxides (*e.g.*, O═C–N at *ca.* 401.1 eV). As displayed in Fig. 2(d), the O 1s spectra can be deconvoluted into two peaks centered at 531.2 eV and 532.0 eV, assigned to the C═O and C–O groups, respectively. XPS spectral analysis reveals that the G-CDs contain abundant hydrophilic functional groups and a high content of doped N, which is in good agreement with the FTIR analysis (Fig. 2).

3.2. Optical properties of G-CDs

The UV-vis absorption spectra and fluorescence spectra were obtained to investigate the optical properties of the G-CDs. The UV-vis absorption spectrum is shown in Fig. 1(d). The observed short-wavelength absorption bands located at 250 nm and 272 nm could be assigned to the $\pi \rightarrow \pi^*$ transition of the aromatic C═C of the sp^2 domain. The long-wavelength absorption bands at 320 nm and 410 nm are generally attributed to the $n \rightarrow \pi^*$ transitions of C═N/C═O and other functional groups of the CDs. Fig. 3 shows the PL spectra of the G-CDs prepared at different reaction temperatures and times. It can clearly be seen from Fig. 3(a) and (b) that with the reaction temperature or time increasing, the emission wavelength of the G-CDs does not fluctuate perceptibly but only varies in the QY (Table S1, ESI†). This indicates that the G-CDs prepared using the microwave solid-phase approach show strong repeatability and a high emission stability. In addition, it was surprisingly found that the stained tissue paper with the G-CDs solution glowed bright green light under excitation of ultraviolet light at 365 nm. Fig. 3(c) compares the discrepancy in the color of the stained tissue paper between illumination with natural light (top) and UV light (bottom) at 365 nm, indicating the strong PL and the great potential of G-CDs in fluorescent ink or anti-counterfeiting applications (Fig. 3).

Fig. 3(d) shows the PL spectra of the G-CDs prepared under the optimal conditions (190 °C, 8 min). The maximum emission is located at 521 nm within the green-light region. With an

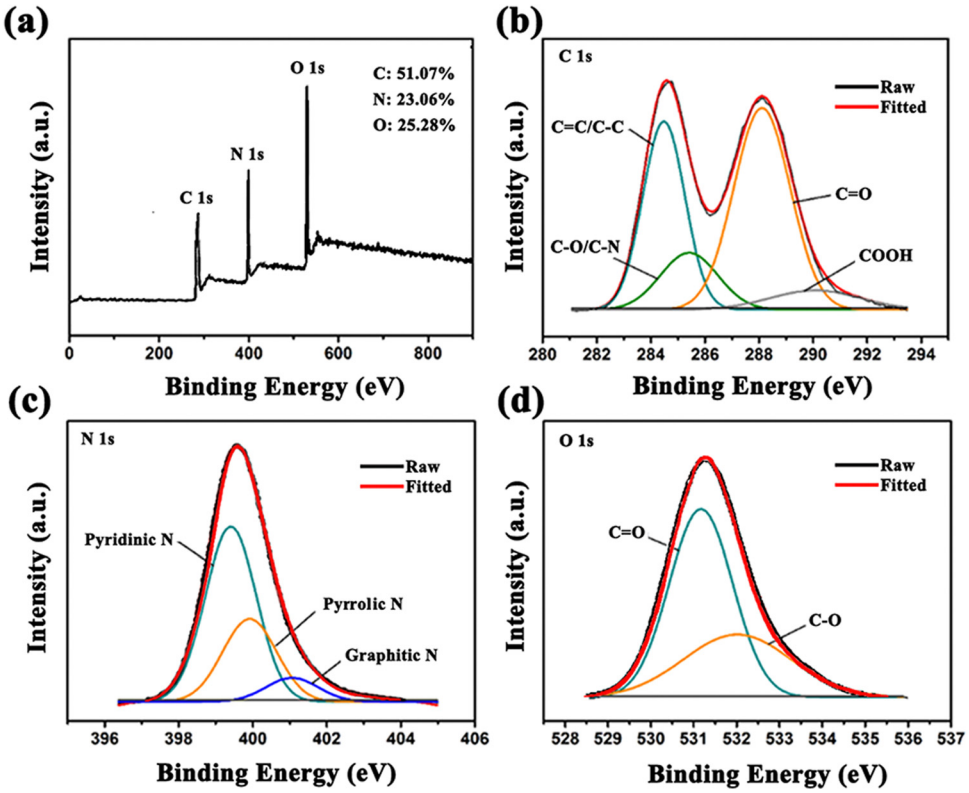

Fig. 2 (a) XPS survey spectra for the prepared G-CDs; magnification and fitting curves of (b) the C1s peak, (c) the N1s peak, and (d) the O1s peak.

increase in the excitation wavelength (from 360 nm to 480 nm), the emission peaks appear to be red-shifted (from 500 nm to 550 nm), suggesting a certain degree of excitation dependence. This may be related to the different defect states and doping effects on the surface of the CDs.[38] The inset in the figure displays the strong green light of the G-CDs under excitation with ultraviolet light. To the best of our knowledge, this is the first report of green-light-emitting CDs prepared using a solid-phase approach, because only the synthesis of blue-light-emitting CDs using a microwave-involved method has been reported so far.[35,36,39] It is well known that fluorescent CDs with a longer wavelength emission have been always pursued by researchers because of their significance for extending the light-absorption ranges and realizing the effective utilization of light. This finding further arouses the confidence of the scientific community to prepare much longer-wavelength fluorescent CDs using efficient one-step solid-state reactions. It is believed that the successful preparation of G-CDs could be attributed to the N dopant in the conjugated carbon nucleus. In the present work, when the nitrogen source (urea) was introduced to and participated in the reaction with the carbon source (citric acid) under microwave irradiation, the emission wavelength of the resulting product was red-shifted significantly from the blue- to the green-light region, as compared with blue-light-emitting CDs with an emission wavelength of 454 nm that were synthesized using a single carbon source as the reactant.[39]

It is indicated that the fluorescence performance of CDs relies intimately on the doping of N. As N is an electron donor entity, its doping may produce new hybridized states located in the existing energy gap between the occupied valence band and the unoccupied conduction band of the conjugated carbon nucleus. Thus, the PL emission of light with a lower photon energy but a long wavelength is possible when excited using high-energy ultraviolet light, which is consistent with previous reports.[40]

Fig. 3(e) shows the PL spectra of the G-CD-based phosphor, and the inset displays the bright green-light-emission of the phosphor under 365 nm ultraviolet light. As can be seen from the spectra, the G-CD-based phosphor exhibits a more stable fluorescence compared with the G-CD dispersion shown in Fig. 3(d). This may be attributed to the starch, which serves as a framework matrix with good dispersion, providing abundant attachment sites for G-CDs to inhibit the non-radiative decay process and photoluminescence quenching induced by aggregation.

Besides, the up-conversion fluorescence characteristics of the G-CDs were observed for the samples. Up-conversion fluorescence has great potential in the field of biological imaging on account of long wavelength excitation light, especially near-infrared light, which causes less damage to biological tissues, has a weak scattering ability, a small spontaneous fluorescence interference and high spatial resolution. As shown in Fig. 3(f), the G-CD emission occurs in the blue and green region under excitation at 660–820 nm (near-infrared excitation), which may find exciting applications in bio-imaging or energy collection.

3.3. Stability of G-CDs

Stability, as a significant factor of materials, plays a vital role for the practical application of CDs. Therefore, the pH stability,

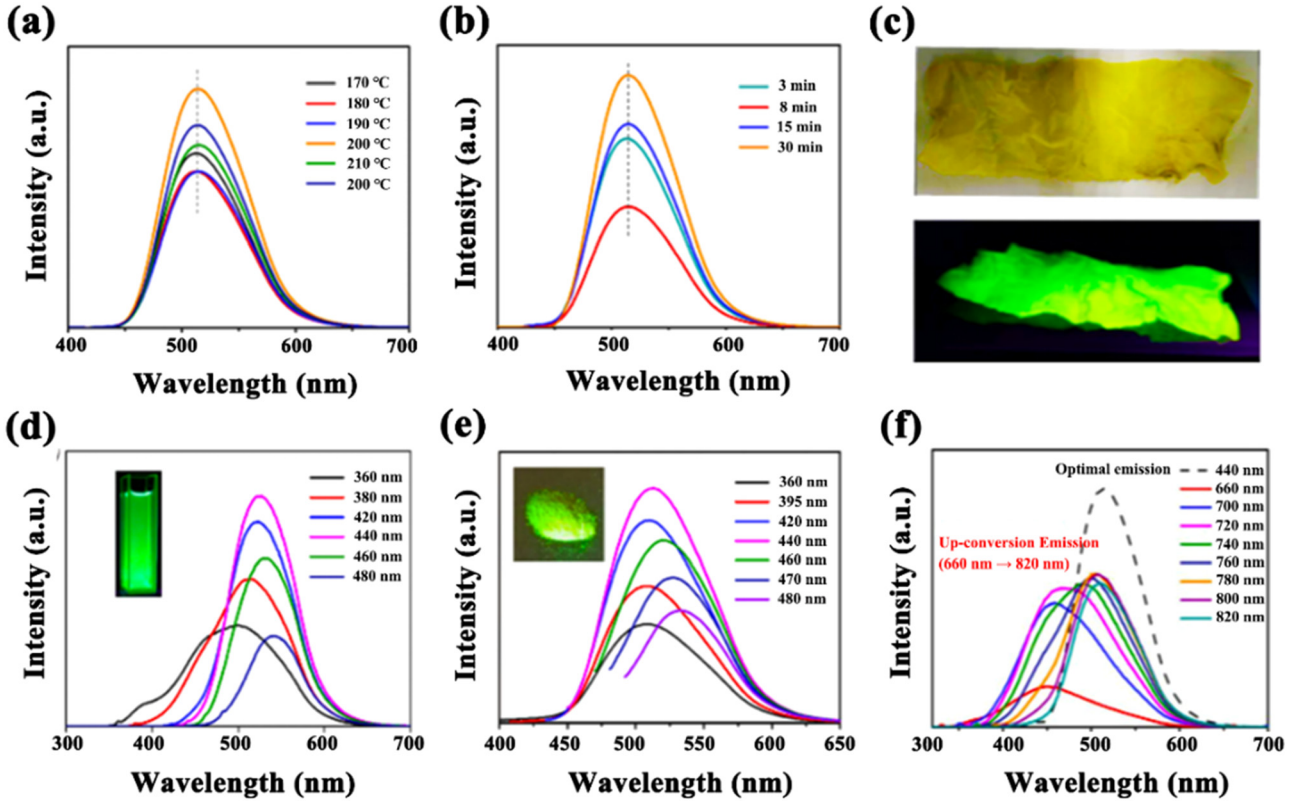

Fig. 3 (a) and (b) PL spectra of G-CDs prepared at different reaction temperatures and times; (c) pictures of tissue paper stained with G-CDs in natural light (top) and when excited at 365 nm (bottom); (d) PL spectra of G-CDs in ethanol solution (inset: illumination using a 365 nm UV lamp); (e) PL spectra of G-CD-based phosphor (inset: illumination using a 365 nm UV lamp); and (f) up-conversion emission spectra of G-CDs.

thermal stability, and long-term storage stability of the G-CDs were studied. G-CDs solution with different pH values were prepared by adding HCl/NaOH (10 mg mL^{-1}) aqueous solution in different volumes. The fluorescence spectra were recorded to assess the stability of the G-CD solutions in different solvent polarities. As can be seen in Fig. 4(a), the fluorescence intensity changed slightly with the increasing pH value of the solution, indicating the good pH stability of the G-CDs. This may be attributed to changes in the surface charge caused by the protonation and deprotonation of surface functional groups (amino, carboxyl). The thermal stability of the G-CDs was assessed by comparing the changes in fluorescence intensity of the PL spectra. It can be seen in Fig. 4(b) that the fluorescence intensities of the G-CDs do not change significantly with the increase in temperature from 20 °C to 70 °C, but intensity decreases slightly at 100 °C. This indicates that G-CDs exhibit good thermal stability over a relatively wide temperature range. Another investigation was conducted to assess the storage stability of the G-CDs. As shown in Fig. 4(c), there is no appreciable change in the fluorescence intensity of the PL spectrum of G-CDs that were stored for one month, demonstrating that the as-prepared G-CDs show a stable fluorescence performance (Fig. 4).

The time-resolved fluorescence decay curve of the G-CD-based phosphor is shown in Fig. 5. The curve was tested under the excitation wavelength of 440 nm and the emission wavelength of 521 nm. The fitting equation is shown in eqn (2):

$$Y(t) = \alpha_1 \exp\left(-t \times {\tau_1}^{-1}\right) + \alpha_2 \exp\left(-t \times {\tau_2}^{-1}\right) \quad (2)$$

where $Y(t)$ represents the individual exponential decay intensities, and α_1 and α_2 are the proportional coefficients of decay time τ_1 and τ_2, respectively. The average fluorescence lifetime (τ_{ave}) of the G-CD-based phosphor can be calculated using eqn (3):

$$\tau_{ave} = \left(\alpha_1 {\tau_1}^2 + \alpha_2 {\tau_2}^2\right) \times \left(\alpha_1 \tau_1 + \alpha_2 \tau_2\right)^{-1} \quad (3)$$

The parameters and calculation results on the basis of eqn (3) are shown in Table 1. The result shows that the average fluorescence lifetime of the G-CD-based phosphor is about 7.93 ns. The fluorescence lifetime of the G-CD-based phosphor consists of short-lived components τ_1 and τ_2, which can be attributed to the intrinsic complexation of the carbon nucleus and surface functional groups, respectively. In this research, the proportional coefficient of α_1 is 61.19%, and the proportional coefficient of α_2 is 38.81%, indicating that the fluorescence emission of the G-CD-based phosphor is dominated by the control of carbon nucleus states.

3.4. G-CDs applied in the detection of Fe^{3+}

Eleven kinds of cations, including Zn^{2+}, Pb^{2+}, Ni^{2+}, Mn^{2+}, Mg^{2+}, K^{+}, Co^{2+}, Cd^{2+}, Ag^{+}, Cu^{2+} and Fe^{3+} were selected to evaluate representatively the effects of cations on the fluorescence of the G-CDs. As exhibited in Fig. 4(d), the fluorescence emission of the CDs could be significantly quenched by Fe^{3+} compared with

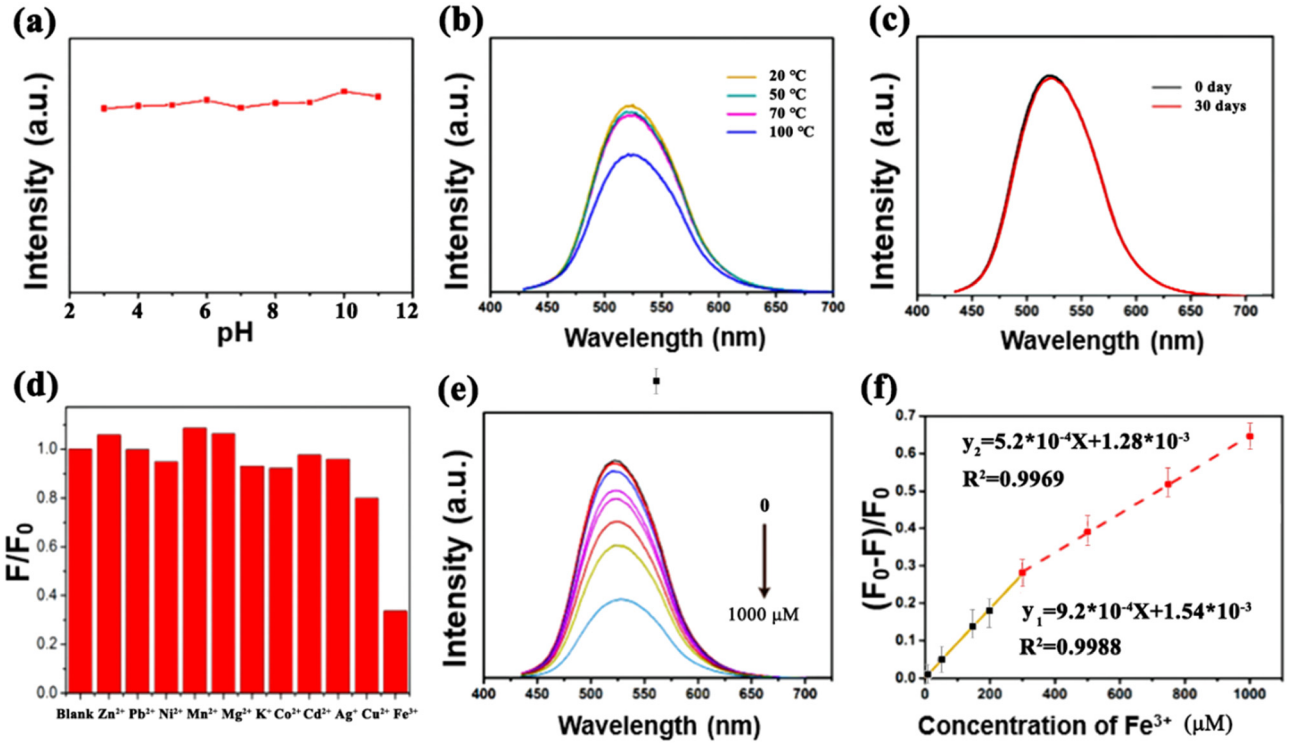

Fig. 4 PL intensity variations of G-CDs (a) at different pH values, (b) measured at different temperatures, and (c) after being stored at room temperature for one month. (d) Histogram of G-CD selectivity for different metal ions, where F_0 and F are the PL intensities of the G-CD dispersion in the absence and presence of different metal ions, respectively; (e) effects of different concentrations of Fe^{3+} on the PL intensity of G-CDs; and (f) linear relationship between $(F_0 - F)/F_0$ and the Fe^{3+} concentration, where F_0 and F are the PL intensities of the G-CD dispersion in the absence and presence of Fe^{3+}, respectively.

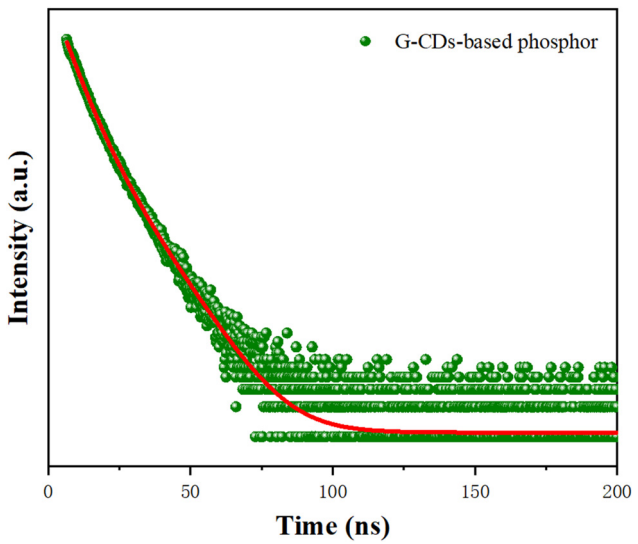

Fig. 5 Time-resolved fluorescence decay curve of the G-CD-based phosphor.

Table 1 Fitting parameters of the G-CD-based phosphor decay curve

α_1 (%)	τ_1 (ns)	α_2 (%)	τ_2 (ns)	τ_{ave} (ns)
61.19	4.96	38.81	10.21	7.93

the other cations. Fluorescence quenching tests of the G-CDs for representative ions of Zn^{2+}, Cu^{2+}, Ni^{2+}, Co^{2+} and Fe^{3+} under UV light are shown in Fig. 6, suggesting the sensitive detection of Fe^{3+} under UV light based on the comparative fluorescence quenching. Therefore, the G-CDs are able to respond to Fe^{3+} selectively in complex cation-containing systems. The quenching effect by Fe^{3+} was attributed to an inner filter caused by its strong absorption at the mentioned excitation wavelength, and the decreased fluorescence of the CDs is due to the complex reaction between the Fe^{3+} ions and −OH groups on the surface of the CDs. With an increase in the Fe^{3+}-ion concentration, the surface defect states of the CDs are significantly changed because of the interaction of more −OH groups with Fe^{3+}, resulting in the PL quenching. The fluorescence intensities of the G-CDs in PBS buffer solutions at pH = 7.4 containing Fe^{3+} at various concentrations were measured to study the detection sensitivity. In Fig. 4(e), the emission of the G-CDs shows a decrease in intensity after adding Fe^{3+} with increasing concentrations from 0 to 1000 μM. The quenching efficiency ($(F_0 - F)/F_0$) of the G-CDs shows two linear regions, in the range of 0–300 μM and for 300–1000 μM. These regions are linearly fitted as $y_1 = 9.2 \times 10^{-4}X + 1.5 \times 10^{-3}$ ($R^2 = 0.9988$) and $y_2 = 5.2 \times 10^{-4}X + 1.28 \times 10^{-3}$ ($R^2 = 0.9969$), respectively, where y is equal to $(F_0 - F)/F_0$, and X represents the concentration of Fe^{3+}. The detection limit was

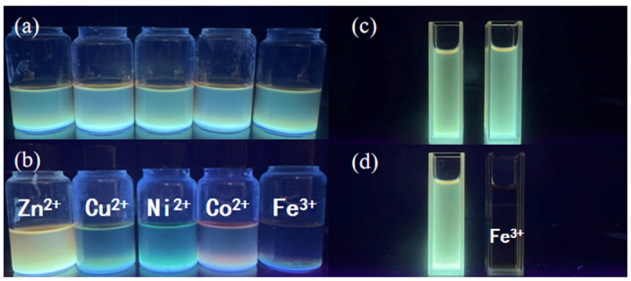

Fig. 6 (a) and (b) Fluorescence sensitivity test of the G-CDs to different heavy metal ions under UV light; and (c) and (d) sensitivity test of the G-CDs against Fe^{3+} fluorescence under UV light.

calculated to be 10 μM. The fluorescence responses of the G-CDs to Zn^{2+}, Pb^{2+}, Ni^{2+}, Mn^{2+}, Mg^{2+}, K^{+}, Co^{2+}, Cd^{2+}, Ag^{+} and Cu^{2+} are negligible compared with that of Fe^{3+}. Therefore, the prepared G-CDs are a potential detector for monitoring the concentration of Fe^{3+} in industrial wastewater (Fig. 6).

3.5. Application of G-CDs in WLEDs

The WLEDs were fabricated *via* coating the G-CD-based phosphor and the red phosphor mixed with epoxy resin directly onto the surface of a commercial 460 nm blue-chip. Efficient white-light emission from the LEDs could be observed under different forward bias currents. The electroluminescence (EL) spectra of the as-fabricated G-CD-based WLEDs were recorded at currents ranging from 20 mA to 120 mA, as shown in Fig. 7(a). They all cover a broad spectral region from 440 nm to 700 nm, each of which showing three clearly distinct peaks, namely the peak at 460 nm corresponding to blue fluorescence from the chip, the one at 540 nm that arises from the G-CD-based phosphor, and the emission at 620 nm that originates from the red phosphor. The relatively strong peak in the red region demonstrates slight reabsorption, which ensures the high CRI of the LEDs. Fig. 7(b) displays the CIE chromaticity diagram of the G-CD-based WLEDs at 100 mA current. The luminous parameters of the G-CD-based WLEDs are shown in Table S2 (ESI†). The CIE chromaticity coordinates are determined as (0.3437, 0.3358), with a CRI of 92.2 and a correlated color temperature (CCT) of 4997 K. These are even comparable to some state-of-the-art commercial WLEDs based on semiconductor CDs and lead halide perovskites. It is believed that G-CD-based phosphors are promising as an alternative to rare-earth-based fluorescent materials for the fabrication of a new generation of light-emitting devices (Fig. 7).

4. Conclusion

In summary, we have developed a facile microwave-assisted solvent-free approach, by which light-emitting CDs with a much longer emission wavelength than ever before were achieved efficiently. The prepared G-CDs present a green-light emission with a maximum emission wavelength of 521 nm when excited at 440 nm. By virtue of the introduction of microwaves, the reaction can be accomplished in a few minutes without the addition of any organic solvent, and the resulting CDs can be obtained with a relatively high production yield and quantum yield of 59.15% and 48.8%, respectively. Besides, G-CDs retain a stable PL performance over a wide range of pH values, at relatively high temperatures, and are suitable for long-term use. Furthermore, the potential of G-CDs in Fe^{3+} detection and WLED devices was explored. G-CDs exhibit the highly sensitive detection of Fe^{3+} with a limit as low as 10 μM. The WLED prototypes fabricated based on these G-CDs favorably emit white light that features a CRI of 92.2 and CIE coordinates of (0.3437, 0.3358), which are comparable to the most desirable white-light emission. The approach developed in this work avoids the use of organic solvents throughout the preparation processes, thus providing an eco-friendly route for the preparation of CDs. Moreover, the microwave-assisted solid-phase reaction that can use a broad range of resources not only facilities the post-treatment but also enables the CDs to be produced at low cost, making it possible for the scaled-up production of CDs. Therefore, the simplified operational procedures, eco-friendly preparation, low cost, high yields, and the favorable fluorescence performance endow the G-CDs with

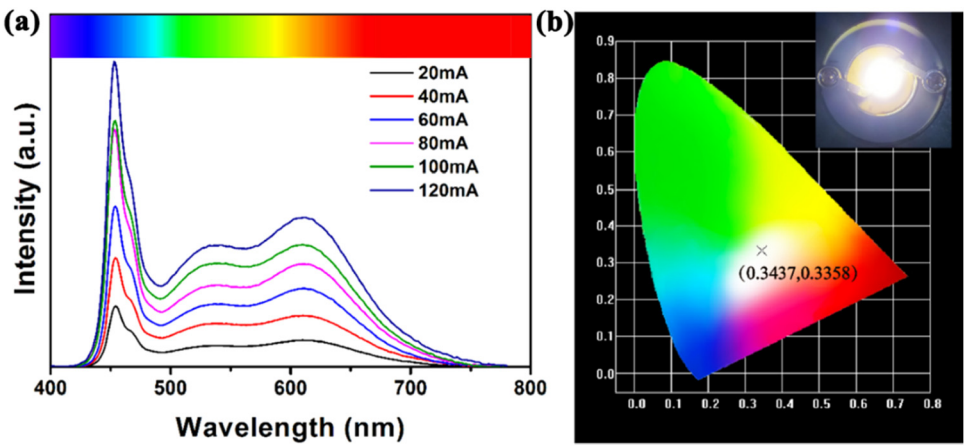

Fig. 7 (a) Emission spectra of the G-CD-based WLEDs at different currents; and (b) CIE chromaticity diagram of the G-CD-based WLEDs at 100 mA current.

great potential in the application of ion-detection chemical sensors, and particularly for the fabrication of high-performance light-emitting devices.

Conflicts of interest

There are no conflicts of interest to declare.

Acknowledgements

The authors are grateful for financial support from the Natural Science Foundation Shanghai, China (Grant No. 18ZR1426300, 17511101603), and the State Key Laboratory of Pollution Control and Resource Reuse Foundation (Grant no. PCRRF19017).

References

1 Y. T. Shen, X. Zhang, L. J. Liang, J. Yue, D. S. Huang, W. Q. Xu, W. Shi, C. Y. Liang and S. P. Xu, *Carbon*, 2020, **156**, 558–567.
2 Y. J. Chung, J. Kim and C. B. Park, *ACS Nano*, 2020, **14**, 6470–6497.
3 Y. Chen, Y. Cao, C. Ma and J. J. Zhu, *Mat. Chem. Front.*, 2020, **4**, 369–385.
4 N. Kottam and S. P. Smrithi, *Methods Appl. Fluoresc.*, 2021, **4**, 24.
5 Y. Li, D. Liu, Y. Q. Wang, F. F. Wang and H. X. Qiu, *Mater. Adv.*, 2021, **2**, 3346–3352.
6 Y. Li, Y. Q. Wang, D. Liu, Y. Gao, S. N. Wang and H. X. Qiu, *ACS Omega*, 2021, **6**(22), 14629–14678.
7 N. Mas, J. L. Hueso, G. Martinez, A. Madrid, R. Mallada, M. C. Ortega-Liebana, C. Bueno-Alejo and J. Santamaria, *Carbon*, 2020, **156**, 453–462.
8 M. Han, S. J. Zhu, S. Y. Lu, Y. B. Song, T. L. Feng, S. Y. Tao, J. J. Liu and B. Yang, *Nano Today*, 2018, **19**, 201–218.
9 G. Q. Hu, Y. Q. Sun, J. L. Zhuang, X. J. Zhang, H. R. Zhang, M. T. Zheng, Y. Xiao, Y. R. Liang, H. W. Dong and H. Hu, *et al.*, *Small*, 2020, **16**, 8.
10 C. X. Guo, H. B. Yang, Z. M. Sheng, Z. S. Lu, Q. L. Song and C. M. Li, *Angew. Chem., Int. Ed.*, 2010, **49**, 3014–3017.
11 L. Guo, J. C. Ge, W. M. Liu, G. L. Niu, Q. Y. Jia, H. Wang and P. F. Wang, *Nanoscale*, 2016, **8**, 729–734.
12 S. Q. Huang, Q. Zhang, P. Y. Liu, S. J. Ma, B. Xie, K. Yang and Y. P. Zhao, *Appl. Catal., B*, 2020, **263**, 12.
13 M. H. Lan, Y. F. Di, X. Y. Zhu, T. W. Ng, J. Xia, W. M. Liu, X. M. Meng, P. F. Wang, C. S. Lee and W. J. Zhang, *Chem. Commun.*, 2015, **51**, 15574–15577.
14 Y. F. Ding, J. X. Zheng, J. L. Wang, Y. Z. Yang and X. G. Liu, *J. Mater. Chem. C*, 2019, **7**, 1502–1509.
15 H. Zhang, H. Q. Zhang, A. Z. Pan, B. Yang, L. He and Y. S. Wu, *Adv. Mater. Technol.*, 2021, **6**, 26.
16 P. He, Y. X. Shi, T. Meng, T. Yuan, Y. C. Li, X. H. Li, Y. Zhang, L. Z. Fan and S. H. Yang, *Nanoscale*, 2020, **12**, 4826–4832.
17 Y. C. Sim, S. H. Lim, Y. S. Yoo, M. H. Jang, S. Choi, H. S. Yeo, K. Y. Woo, S. Lee, H. G. Song and Y. H. Cho, *Nanoscale*, 2018, **10**, 4686–4695.
18 N. A. Travlou, D. A. Giannakoudakis, M. Algarra, A. M. Labella, E. Rodriguez-Castellon and T. J. Bandosz, *Carbon*, 2018, **135**, 104–111.
19 Z. M. Markovic, M. Labudova, M. Danko, D. Matijasevic, M. Micusik, V. Nadazdy, M. Kovacova, A. Kleinova, Z. Spitalsky and V. Pavlovic, *et al.*, *ACS Sustainable Chem. Eng.*, 2020, **8**, 16327–16338.
20 Y. H. Liu, W. X. Duan, W. Song, J. J. Liu, C. L. Ren, J. Wu, D. Liu and H. L. Chen, *ACS Appl. Mater. Interfaces*, 2017, **9**, 12663–12672.
21 X. Y. Xu, R. Ray, Y. L. Gu, H. J. Ploehn, L. Gearheart, K. Raker and W. A. Scrivens, *J. Am. Chem. Soc.*, 2004, **126**, 12736–12737.
22 J. G. Zhou, C. Booker, R. Y. Li, X. T. Zhou, T. K. Sham, X. L. Sun and Z. F. Ding, *J. Am. Chem. Soc.*, 2007, **129**, 744–745.
23 S. L. Shen, J. J. Wang, Z. J. Wu, Z. Du, Z. H. Tang and J. H. Yang, *Nanomaterials*, 2020, **10**, 11.
24 Y. P. Sun, B. Zhou, Y. Lin, W. Wang, K. A. S. Fernando, P. Pathak, M. J. Meziani, B. A. Harruff, X. Wang and H. F. Wang, *et al.*, *J. Am. Chem. Soc.*, 2006, **128**, 7756–7757.
25 H. T. Li, X. D. He, Y. Liu, H. Huang, S. Y. Lian, S. T. Lee and Z. H. Kang, *Carbon*, 2011, **49**, 605–609.
26 S. Y. Park, H. U. Lee, E. S. Park, S. C. Lee, J. W. Lee, S. W. Jeong, C. H. Kim, Y. C. Lee, Y. S. Huh and J. Lee, *ACS Appl. Mater. Interfaces*, 2014, **6**, 3365–3370.
27 Y. L. Liu, Q. X. Zhou, Y. Y. Yuan and Y. L. Wu, *Carbon*, 2017, **115**, 550–560.
28 F. L. Yuan, P. He, Z. F. Xi, X. H. Li, Y. C. Li, H. Z. Zhong, L. Z. Fan and S. H. Yang, *Nano Res.*, 2019, **12**, 1669–1674.
29 Q. L. Wang, H. Z. Zheng, Y. J. Long, L. Y. Zhang, M. Gao and W. J. Bai, *Carbon*, 2011, **49**, 3134–3140.
30 H. Ding, S. B. Yu, J. S. Wei and H. M. Xiong, *ACS Nano*, 2016, **10**, 484–491.
31 J. X. Zheng, X. H. Liu, Y. Z. Yang, X. G. Liu and B. S. Xu, *New Carbon Mater.*, 2018, **33**, 276–287.
32 Y. Q. Zhang, P. Zhuo, H. Yin, Y. Fan, J. H. Zhang, X. Y. Liu and Z. Q. Chen, *ACS Appl. Mater. Interfaces*, 2019, **11**, 24395–24403.
33 C. Liu, R. J. Wang, B. Wang, Z. Q. Deng, Y. Z. Jin, Y. J. Kang and J. C. Chen, *Microchim. Acta*, 2018, **185**, 8.
34 S. Sun, L. Zhang, K. Jiang, A. G. Wu and H. W. Lin, *Chem. Mater.*, 2016, **28**, 8659–8668.
35 Y. Wang, Q. F. Zhuang and Y. N. Ni, *Chem. – Eur. J.*, 2015, **21**, 13004–13011.
36 M. Cao, Y. Li, Y. Z. Zhao, C. Y. Shen, H. Y. Zhang and Y. F. Huang, *RSC Adv.*, 2019, **9**, 8230–8238.
37 C. Wang, T. T. Hu, Y. Y. Chen, Y. L. Xu and Q. J. Song, *ACS Appl. Mater. Interfaces*, 2019, **17**, 22332–22338.
38 A. Kundu, B. Park, J. Oh, K. V. Sankar, C. Ray, W. S. Kim and S. C. Jun, *Carbon*, 2020, **156**, 110–118.
39 Q. F. Zhuang, Y. Wang and Y. N. Ni, *Luminescence*, 2016, **31**, 746–753.
40 L. Jiang, H. H. Ding, M. S. Xu, X. L. Hu, S. L. Li, M. Z. Zhang, Q. Zhang, Q. Y. Wang, S. Y. Lu and Y. P. Tian, *et al.*, *Small*, 2020, **16**, 9.